Crystal structure and magnetic properties of the layered van der Waals compound VBr_3

Tai Kong, Shu Guo, Danrui Ni, Robert J. Cava

Department of Chemistry, Princeton University, Princeton, New Jersey 08544

KEYWORDS: van der Waals, magnetism, crystal structure

Abstract

Single crystals of the layered, van der Waals compound VBr_3 were synthesized by a vapor transport technique, and characterized by single crystal x-ray diffraction, temperature- and field-dependent magnetization, and temperature-dependent specific heat measurements. VBr_3 has a honeycomb-based BiI_3-type structure with space group *R*-3 (No. 148) at 100 K; analogous to the structure of other honeycomb trihalides. Structural stacking faults were observed as evidenced by the streaking of reflections along *c** in the diffraction data. VBr_3 goes through a structural phase transition at 90.4 K and a subsequent antiferromagnetic phase transition at 26.5 K, below which the magnetic moments are primarily aligned along the *c*-axis.

Introduction

Binary transition metal trihalides have been known for several decades and used as model systems for the study of magnetism in layered compounds[1,2]. This interest has been revived recently through the experimental observation of a monolayer ferromagnet, [3,4] possible due to the van der Waals type crystalline structure of these materials, which makes them favorable for cleaving and subsequent heterostructure fabrication. The magnetic properties of $RuCl_3$ are also of recent interest as promising system to study the Kitaev model[5]. Despite the fact that many binary halides are known, their actual crystal structures and physical properties have not been fully characterized[1]. Among these poorly characterized compounds, the recent rediscovery of ferromagnetism in VI_3 has been of interest as it expands the available ferromagnetic halides beyond CrI_3[6–8]. For the chromium trihalides, both bromide and iodide are ferromagnetic, with CrI_3 having a higher phase transition temperature[1,7,9]. Vanadium trihalides (vanadium neighbors chromium in the periodic table) share many structural similarities with the chromium family, and thus are of interest for the systematic characterization of their crystal structures and magnetic properties. In this paper, we focus on VBr_3.

VBr_3 was reported to exist in a *R*-3 crystal structure[10,11], but no detailed crystal structure is reported in the International Crystal Structure Database (ICSD). In terms of magnetism, VBr_3 was briefly mentioned to order antiferromagnetically at 35 K with an effective moment of 2.29 μ_B/V at room temperature[12]. Further, it is a reported semiconductor with an optical band gap of slightly larger than 1 eV[13]. In this paper, we present a detailed crystal structure determination at 100 K via single crystal x-ray diffraction, and physical property characterization via temperature- and field-dependent magnetization and specific heat measurements.

Experimental

VBr_3 single crystals were synthesized by using the vapor transport technique. The as-received vanadium bromide (III) from Alfa Aesar was in fact nearly pure VBr_2O. Starting materials of VBr_2O and VO (Alfa Aesar) were mixed in a 1:1 molar ratio in an argon glove box, and sealed in a silica tube under vacuum. The VO acts as a reducing agent, forming V_2O_3 during the crystal growth process. The silica tube was placed in a horizontal tube furnace with the hot end kept at 480 °C and the cold end kept close to the edge of the tube furnace. Typical vapor transport

growth took 4 days. Dark, soft, plate-like single crystals of VBr_3 were collected at cold end of the tube. The vapor pressures of VBr_3 and the vanadium oxybromides (VBr_2O and VBrO) are different, which makes the growth of VBr_3 singles crystals possible out of an oxygen-containing environment. A small amount of yellow VBrO can sometimes be found at the cold end of the silica tube, and can be easily detached from the dark VBr_3 single crystals mechanically. VBr_3 single crystals are air-sensitive, similar to VI_3, and thus are handled inside of the glove box as much as possible. Attempts to measure the resistivity of VBr_3 with silver paint and platinum wires were not successful at room temperature due to the extremely large resistance of the material. This is consistent with the semiconducting nature of VBr_3[13].

The reported crystal structure of VBr_3 was confirmed and refined by single-crystal x-ray diffraction. The diffraction data were collected at 100 K on a single crystal with a Kappa Apex2 CCD diffractometer (Bruker) using graphite-monochromated Mo-Kα radiation (λ = 0.71073 Å). The raw data were corrected for background, polarization, and Lorentz factor and multi-scan absorption corrections were applied. Finally, the structure was analyzed by the Intrinsic Phasing method provided by the ShelXT structure solution program[14] and refined using the ShelXL least-squares refinement package with the Olex2 program[15]. The ADDSYM algorithm in program PLATON was used to double check for possible higher symmetry[16].

Both magnetization and specific heat data were measured using a Quantum Design (QD) physical property measurement system (PPMS) Dynacool. Anisotropic magnetization was measured using the vibrating sample magnetometer (VSM) function from 1.8-300 K and from 0-90 kOe. Single crystalline samples were manually aligned in preferred orientation in a plastic capsule provided by QD. The applied field for the temperature dependent measurements was 90 kOe, and magnetic susceptibility is defined as M/H. Zero-field specific heat data were measured down to 1.8 K using the two-tau relaxation method on a collection of single crystals.

Results and discussion

The crystal structure of VBr_3 measured at 100 K is schematically shown in Fig 1. Similar to VI_3[6], VBr_3 has a BiI_3-type honeycomb layer structure, space group *R*-3, No.148. In this structure, VBr_6 octahedra are connected via edge-sharing within each plane, forming a honeycomb lattice, and are separated by a van der Waals gap in between planes. Each V–Br octahedron is only slightly

distorted. As shown in Fig1c, the vanadium atom is slightly displaced from the center of the octahedron along the *c*-axis, causing a minimal difference in V–Br bond lengths: 2.53 and 2.54 Å. Detailed crystal structure information can be found in Table 1 and Table 2.

In the structure of VBr_3, the vanadium atoms are found in two sites. The majority of the vanadium atoms form a honeycomb lattice, similar to many other transition metal trihides, such as CrI_3, VI_3, and $TiCl_3$[1]. The central normally vacant site in the honeycomb lattice is occupied in a minor but not insignificant fashion in the average structure, which if the occupancy was not due to stacking faults, would lead to a triangular lattice such as in VBr_2 if fully occupied[17]. We attribute this partial occupancy in the average structure not to actual site occupancy in the honeycomb layer but to the presence of stacking faults as is commonly seen in van der Waals layered materials. In the case of VI_3, these stacking faults are the reason for the 4% average occupancy of the central atom site in the honeycomb[6]. In the case of VBr_3, however, the stacking faults are found at a much larger fraction (Table 2). This can be illustrated by the comparison of diffraction patterns in *k*-space for VI_3 and VBr_3, shown in Fig 2. It is clear that the VI_3 sample gives "cleaner" spot-like diffraction peaks, showing little streaking. In contrast, VBr_3 shows both twinning and the streaking of reflections along c^* that is characteristic of layered materials with stacking faults[18]. The twining can be accounted for during crystal structure refinement, and the streaking gives rise to the partial occupancy of the central atom site in the average structure, because the streaking comes from local deviations of the stacking sequence from A-B-C to more complex non-A-B-C forms. This kind of streaking pattern appears to all of the VBr_3 samples that were measured. During crystal structure refinements, the stacking faults lead to a significant scattering density in the ideally vacant centers (the V2 sites) of the V-based honeycombs (the V1 sites). Hence, to specify the crystal structure averaged over the honeycomb layers and the stacking fault layers, vanadium was introduced into our crystal structure refinement in the V2 site. Unconstrained refinement of the occupancies of the V1 and V2 sites leads to 0.864(10) and 0.312(19) respectively, which adds up to only $V_{1.02}Br_3$, within error of VBr_3. Thus for the final structural model, the sum of the V1+V2 occupancies was constrained to yield the formula VBr_3; a fully V^{3+} material.

It is worth noting that this stacking fault, or stacking sequence disorder, also occurs in other transition metal trihalide systems such as in $RuCl_3$[19]. In VBr_3, such stacking faults, although

present in significant amounts, do not seem to affect the magnetic and structural phase transition temperatures, as was observed in $RuCl_3$[20]. As will be discussed in the following sections, both magnetic and structural phase transitions of VBr_3 are clear and sharp. Elemental analysis was conducted on several pieces of VBr_3 single crystals. A typical scanning electron microscopy (SEM) image is shown in Fig. 1b. In the SEM image, clear terraces can be observed for this layered material, with the *c*-axis perpendicular to the flat surfaces. Elemental analysis yields a Br to V ratio of 2.9±0.2, which is consistent with single crystal diffraction refinement result.

Now we look into the magnetic properties of VBr_3. Fig. 3 shows its temperature- and field-dependent magnetization. The magnetic susceptibility diverges as temperature decreases, indicating a clear Curie-Weiss behavior, due to the vanadium magnetic moments. In the paramagnetic state, the magnetization is weakly anisotropic with fitted Curie-Weiss temperatures of Θ_c = -20 K and Θ_{ab} = 1 K. The difference in anisotropic Curie-Weiss temperatures, albeit small, may reflect competition between in-plane and out-of-plane magnetic interactions. The effective moment was determined to be approximately 2.6 μ_B/V by fitting from 150 to 300 K, which is close to the expected value of a spin-1 vanadium atom (2.8 μ_B/V), i.e. the formally V^{3+} in VBr_3.

There are two phase transitions observable in the temperature-dependent magnetization data. The higher temperature phase transition appears at ~ 88 K. The magnetization for both H//*c* and H//*ab* dips slightly at the phase transition. For H//c, the feature is stronger than that in H//*ab*. This is similar to the case in VI_3. It is possible that the feature in the H//*ab* data comes from a small misalignment of the sample being measured. This high-temperature phase transition may be of a structural origin. At lower-temperature, ~ 30 K, there is another phase transition. Both magnetization values drop at this phase transition, which suggests that the transition is due to the onset of an antiferromagnetic phase at lower temperature. The magnetization value for H//c decreases significantly more than that for H//ab, suggesting that the vanadium magnetic moments have a larger *c*-axis component in the ordered state. Both phase transitions barely shift in temperature upon the application of axial magnetic field up to 9 T. More detailed neutron scattering measurements are needed to determine the detailed magnetic structure of VBr_3 at low temperature.

The isothermal magnetization data shown in Fig 3b is consistent with the temperature-dependent data. At room-temperature, the data show a clear paramagnetic behavior. Below the structural phase transition, at 50 K, the magnetic anisotropy remains small, consistent with a paramagnetic state in this temperature range. Below the magnetic phase transition temperature, at 1.8 K, magnetic anisotropy develops, with both values at 90 kOe much smaller than the expected saturation moment of a vanadium spin-1 system (2 μ_B/V), implying that more metamagnetic phase transitions may occur at higher applied magnetic fields.

To identify the bulk nature of both phase transitions, we also characterized the specific heat of VBr_3, as shown in Fig. 4. Consistent with magnetic measurements, we observed two clear phase transitions in the zero-field, temperature-dependent specific heat data, at 90.4 K and 26.5 K. The magnetic phase transition temperature (T_N) determined in this study is smaller than the previously reported one of 35 K[12]. The estimated Debye temperature for VBr_3 is about 157 K, larger than that of VI_3 (143 K), which is consistent with the relative molecular weights of the two compounds. The numerical difference in the Debye temperatures, however, is smaller than expected based on a simple Debye model.

Comparing VBr_3 to VI_3[6], the structural phase transition temperature (T_s) is higher while the magnetic phase transition temperature is lower (Fig. 4). The T_N of VBr_3 is close to that observed for VBr_2 at 29.5 K[17]. The structural phase transition of VBr_3 at 90.4 K has not been previously reported. Unfortunately, we were not able to obtain the crystal structure below 90.4 K due to our experimental limitations. Additional study would be needed to reveal the low temperature crystal structure.

Conclusion

We have reported the single crystal growth, crystal structure and magnetic characterization of the layered van der Waals compound VBr_3. Single crystal x-ray diffraction refinement of the average structure indicates that VBr_3 has a BiI_3-type structure (space group R-3, No.148) above 90.4 K. VBr_3 goes through two phase transitions that are both sharp: one that is likely a structural phase transition at 90.4 K and a lower temperature magnetic phase transition at 26.5 K, which is likely an antiferromagnetic phase transition below which the magnetic moment primarily aligns along the *c*-axis. The stacking fault disorder does not broaden these transitions substantially in

temperature. The magnetization and heat capacity measurements are consistent in the identification of these two bulk phase transitions. Future detailed studies may be of interest to reveal the low temperature crystal structure and magnetic structure of VBr_3.

Supporting Information.

CIF files for VBr_3.

Accession Codes

CCDC number 1934916 contain the supplementary crystallographic data for this paper. This data can be obtained free of charge via www.ccdc.cam.ac.uk/data_request/cif, or by emailing data_request@ccdc.cam.ac.uk, or by contacting The Cambridge Crystallographic Data Centre, 12 Union Road, Cambridge CB2 1EZ, UK; fax: + 441223336033.

ORCID

Shu Guo: 0000-0002-2098-8904

Acknowledgments Crystallographic aspects of this work were supported as part of the Institute for Quantum Matter, an Energy Frontier Research Center funded by the U.S. Department of Energy, Office of Science, Basic Energy Sciences under Award No. DE-SC0019331. DN was supported by the ARO MURI on topological insulators, grant W911NF-121-0461. The crystal growth and magnetic property characterization were supported by the Gordon and Betty Moore Foundation, EPiQS initiative, grant GBMF-4412.

Figure Captions:

Figure 1. (a) Schematic drawing of the crystal structure of VBr_3. Central orange atoms are vanadium and dark spheres represent bromine atoms. The area of white color on the vanadium sites represents the percentage of vacancies on that site. (b) shows a SEM image of a VBr_3 single crystal. The orange scale bar in the left corner indicates 50 μm in length. (c) shows a VBr_6 octahedron with V-Br bond distance labeled on the side.

Figure 2. Comparison of the observed single crystal x-ray diffraction patterns for crystals of VBr_3 and VI_3 in two different reciprocal lattice planes (*hk0* and *0kl*).

Figure 3. (a) Anisotropic magnetization of VBr_3 measured at 90 kOe. Inset shows the zoom-in view of the structural phase transition at ~ 90 K. (b) Anisotropic magnetic isotherms measured at 300 K (solid lines), 50 K (open symbols) and 1.8 K (solid symbols).

Figure 4. Zero-field, temperature-dependent specific heat of VBr_3. The dashed line represents the zero-field specific heat data[6] from VI_3 for comparison.

Figure 1

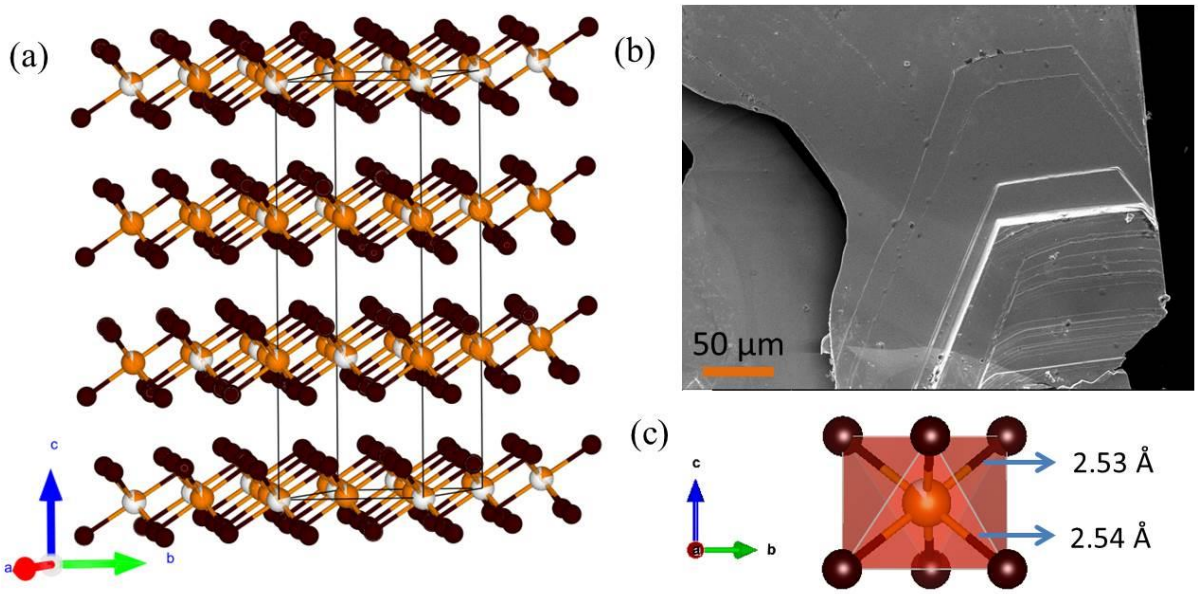

Figure 2

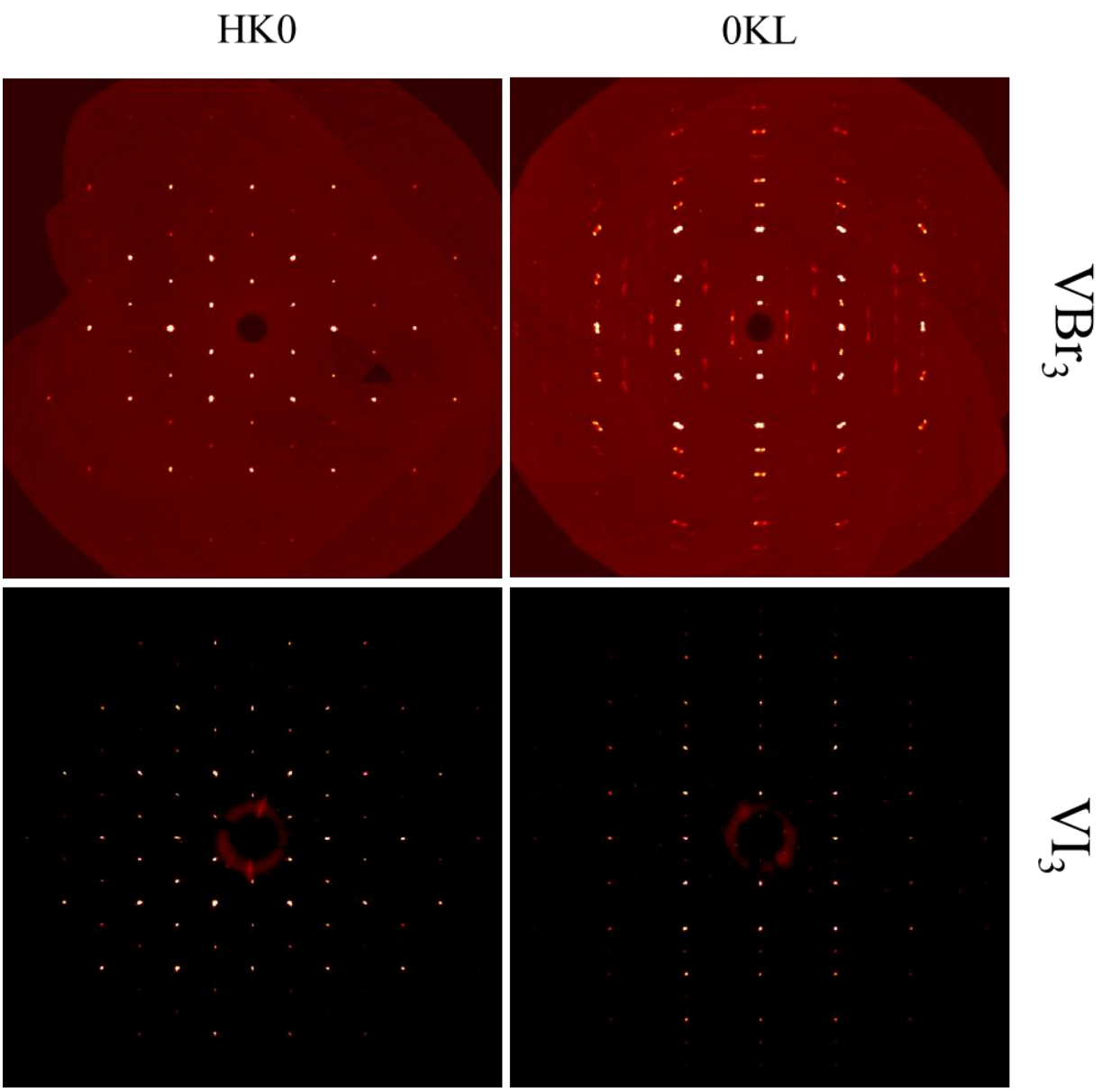

Figure 3

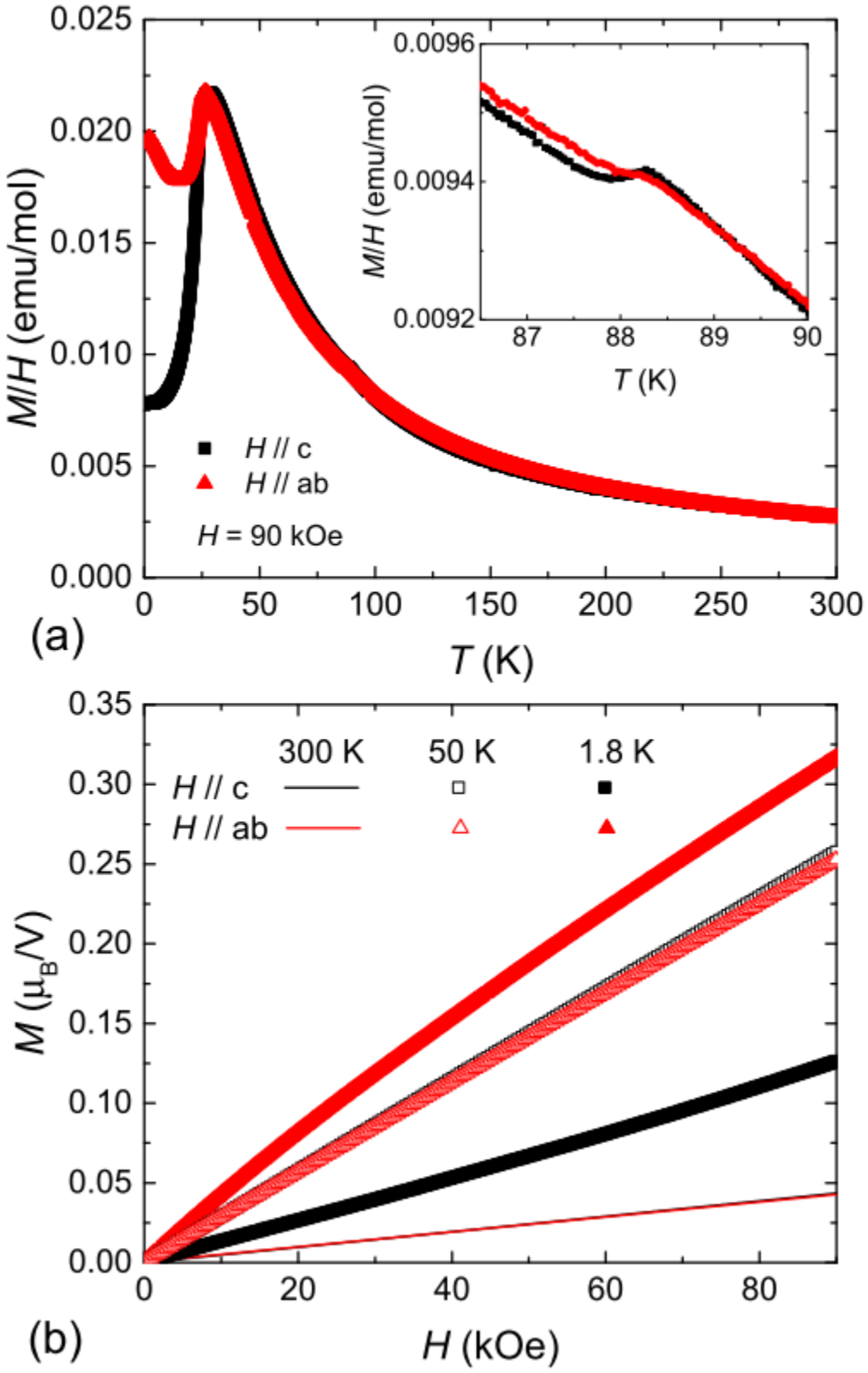
0.025
0.020
0.015
0.010
0.005
0.000
M/H (emu/mol)
0
50
100
150
200
250
300
T (K)
(a)
H // c
H // ab
H = 90 kOe
0.0096
0.0094
0.0092
M/H (emu/mol)
87
88
89
90
T (K)
0.35
0.30
0.25
0.20
0.15
0.10
0.05
0.00
M (μB/V)
300 K
50 K
1.8 K
H // c
H // ab
0
20
40
60
80
H (kOe)
(b)

Figure 4

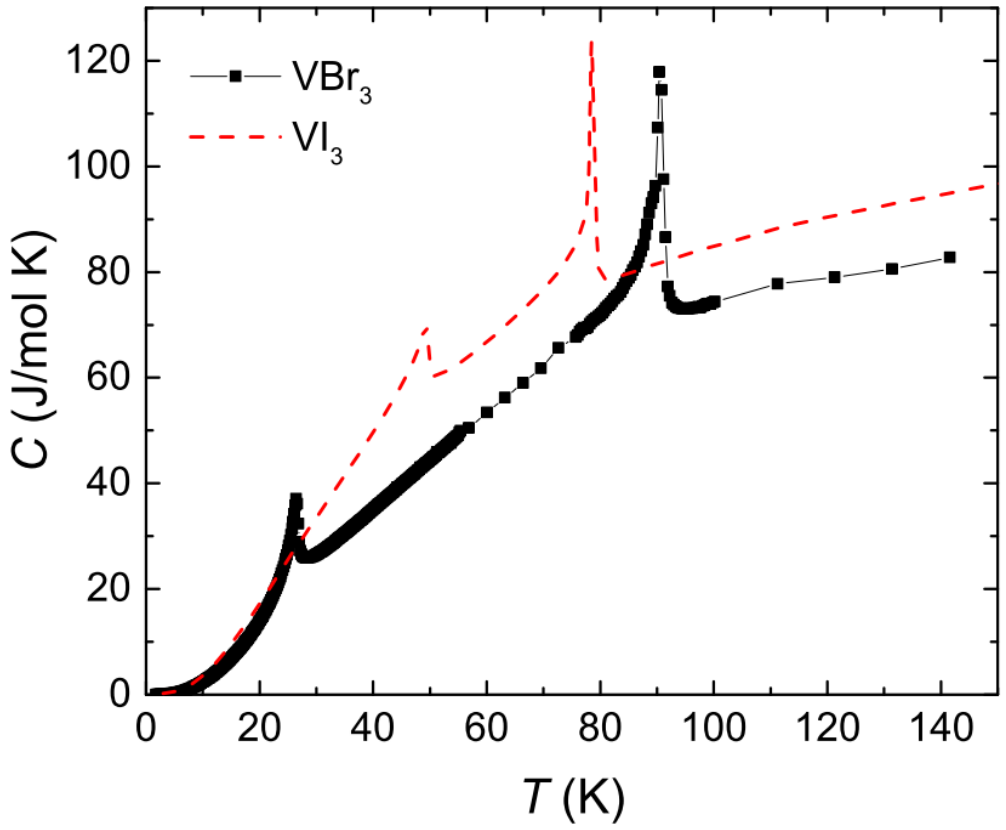

Table 1. Crystallographic Data for VBr_3 at 100 K.

T (K)	100(1)
formula mass(amu)	290.67
crystal system	trigonal
space group	*R*-3 (No.148)
a(Å)	6.3711(5)
c(Å)	18.3763(16)
V(Å^3)	645.98(9)
Z	6
ρ*(calcd)(g/cm^3)*	4.483
λ (Å)	0.71073
F(000)	768
θ*(deg)*	3.33-27.46
Cryst size (mm^3)	0.032 × 0.076 × 0.194
μ(mm^{-1})	29.908
Final R indices (R_1/ωR_2)	0.0368/0.0635
R indices (all data) (R_1/ωR_2)	0.0467/0.0666
Residual electron density/ (eÅ^{-3})	(-1.671) - 1.630
Goodness of fit	1.166

Table 2. Wyckoff positions, coordinates, occupancies, and equivalent isotropic displacement parameters respectively for VBr_3 at 100 K.

Atoms	Wyck.Site	x	y	z	S.O.F.	U_{eq}
V1	6*c*	0	0	0.33345(15)	0.897(4)	0.0050(5)
V2	3*a*	0	0	0	0.207(8)	0.0050(5)
Br1	18*f*	0.34914(14)	0.00106(15)	0.07924(4)	1	0.0081(2)

References

(1) McGuire, M. A. Crystal and Magnetic Structures in Layered, Transition Metal Dihalides and Trihalides. *Crystals* **2017**, *7* (5), 121.

(2) *Magnetic Properties of Layered Transition Metal Compounds*; de Jongh, L. J., Ed.; Physics and Chemistry of Meterials with Low-Dimensional Structures; Springer Netherlands: Dordrecht, 1990; Vol. 9.

(3) Gong, C.; Li, L.; Li, Z.; Ji, H.; Stern, A.; Xia, Y.; Cao, T.; Bao, W.; Wang, C.; Wang, Y.; et al. Discovery of Intrinsic Ferromagnetism in Two-Dimensional van Der Waals Crystals. *Nature* **2017**, *546* (7657), 265–269.

(4) Huang, B.; Clark, G.; Navarro-Moratalla, E.; Klein, D. R.; Cheng, R.; Seyler, K. L.; Zhong, D.; Schmidgall, E.; McGuire, M. A.; Cobden, D. H.; et al. Layer-Dependent Ferromagnetism in a van Der Waals Crystal down to the Monolayer Limit. *Nature* **2017**, *546*, 270--.

(5) Sears, J. A.; Songvilay, M.; Plumb, K. W.; Clancy, J. P.; Qiu, Y.; Zhao, Y.; Parshall, D.; Kim, Y.-J. Magnetic Order in α-RuCl 3 : A Honeycomb-Lattice Quantum Magnet with Strong Spin-Orbit Coupling. *Phys. Rev. B* **2015**, *91*, 144420.

(6) Kong, T.; Stolze, K.; Timmons, E. I.; Tao, J.; Ni, D.; Guo, S.; Yang, Z.; Prozorov, R.; Cava, R. J. VI 3 —a New Layered Ferromagnetic Semiconductor. *Adv. Mater.* **2019**, *31* (17), 1808074.

(7) Son, S.; Coak, M. J.; Lee, N.; Kim, J.; Kim, T. Y.; Hamidov, H.; Cho, H.; Liu, C.; Jarvis, D. M.; Brown, P. A. C.; et al. Bulk Properties of the van Der Waals Hard Ferromagnet VI3. *Phys. Rev. B* **2019**, *99*, 041402.

(8) Tian, S.; Zhang, J.-F.; Li, C.; Ying, T.; Li, S.; Zhang, X.; Liu, K.; Lei, H. Ferromagnetic van Der Waals Crystal VI3. *J. Am. Chem. Soc* **2019**, *141*, 42.

(9) McGuire, M. A.; Dixit, H.; Cooper, V. R.; Sales, B. C. Coupling of Crystal Structure and Magnetism in the Layered, Ferromagnetic Insulator CrI3. *Chem. Mater.* **2015**, *27* (2), 612–620.

(10) Klemm, W.; Hoschek, E. Magnetochemische Untersuchungen. XX. Über Das Magnetische Verhalten Einiger Einfacher Vanadinverbindungen. *Zeitschrift für Anorg. und Allg. Chemie* **1936**, *226* (4), 359–369.

(11) McCarley, R. E.; Roddy, J. W.; Berry, K. O. Transport Reactions of Some Vanadium(III) Halides. Mixed Halide Formation. *Inorg. Chem.* **1964**, *3* (1), 50–54.

(12) Wilson, J. A.; Maule, C.; Strange, P.; Tothill, J. N. Anomalous Behaviour in the Layer Halides and Oxyhalides of Titanium and Vanadium: A Study of Materials Close to Delocalisation. *J. Phys. C* **1987**, *20*, 4159–4167.

(13) Maulet, C. H.; Tothill$, J. N.; Strange, P.; Wilson, J. A. An Optical Investigation into the 3d1 and 3d2 Transition-Metal Halides and Oxyhalides, Compounds near to Delocalisation. *J. Phys. C Solid State Phys* **1988**, *21*, 2153–2179.

(14) Sheldrick, G. M. Crystal Structure Refinement with SHELXL. *Acta Crystallogr C* **2015**, *71* (1), 3–8.

(15) Dolomanov, O. V; Bourhis, L. J.; Gildea, R. J.; Howard, J. A. K.; Puschmann, H. OLEX2: A Complete Structure Solution, Refinement and Analysis Program. *J. Appl. Cryst* **2009**, *42*, 339–341.

(16) Spek, A. L. Single-Crystal Structure Validation with the Program PLATON. *J. Appl. Cryst* **2003**, *36*, 7–13.

(17) Kinshiro, H.; Hiroaki, K.; Koji, U. Study of Frustration Effects in Two-Dimensional Triangular Lattice Antiferromagnets–Neutron Powder Diffraction Study of VX2, X≡Cl, Br and I. *J. Phys. Soc. Japan* **1983**, *52* (5), 1814–1824.

(18) *Crystallography and Crystal Chemistry of Materials with Layered Structures*; Lévy, F., Ed.; Springer Netherlands: Dordrecht, 1976.

(19) Johnson, R. D.; Williams, S. C.; Haghighirad, A. A.; Singleton, J.; Zapf, V.; Manuel, P.; Mazin, I. I.; Li, Y.; Jeschke, H. O.; Valentí, R.; et al. Monoclinic Crystal Structure of Alpha-RuCl3 and the Zigzag Antiferromagnetic Ground State. *Phys. Rev. B* **2015**, *92* (23), 235119.

(20) Cao, H. B.; Banerjee, A.; Yan, J.-Q.; Bridges, C. A.; Lumsden, M. D.; Mandrus, D. G.; Tennant, D. A.; Chakoumakos, B. C.; Nagler, S. E. Low-Temperature Crystal and Magnetic Structure of RuCl3. *Phys. Rev. B* **2016**, *93* (13), 134423.